Highly active, robust and reusable micro-/mesoporous TiN/Si3N4 nanocomposite-based catalysts for clean energy: Understanding the key role of TiN nanoclusters and amorphous Si3N4 matrix in the performance of the catalyst system

Abhijeet Lale, Maira Debarba Mallmann, Shotaro Tada, Alina Bruma, Saim Özkar, Ravi Kumar, Masaaki Haneda, Ricardo Antonio Francisco Machado, Yuji Iwamoto, Umit Demirci, et al.

Highly Active, Robust and Reusable Micro-/Mesoporous TiN/Si$_3$N$_4$ Nanocomposite-based Catalysts for Clean Energy: Understanding the Key Role of TiN Nanoclusters and Amorphous Si$_3$N$_4$ Matrix in the Performance of the Catalyst System

Abhijeet Lale[a]*, Maira Debarba Mallmann[a,b], Shotaro Tada[c], Alina Bruma[d], Saim Özkar[e], Ravi Kumar[f], Masaaki Haneda[d], Ricardo Antonio Francisco Machado[b], Yuji Iwamoto[c], Umit B. Demirci[g], and Samuel Bernard[a]*

(a) Univ. Limoges, CNRS, IRCER, UMR 7315, F-87000, Limoges, France

(b) Chemical Engineering, Federal University of Santa Catarina, 88010-970 Florianópolis, Brazil

(c) Nagoya Inst Technol, Grad Sch Engn, Dept Frontier Mat, Showa Ku, Nagoya, Aichi 4668555, Japan

(d) National Institute of Standards and Technology, Maryland, USA

(e) Department of Chemistry, Middle East Technical University, 06800 Ankara, Turkey

(f) Laboratory for High Performance Ceramics, Department of Metallurgical and Materials Engineering, Indian Institute of Technology-Madras (IIT Madras), Chennai 600036, India.

(g) IEM (Institut Europeen des Membranes), UMR 5635 (CNRS-ENSCM-UM), Universite Montpellier, Place E. Bataillon, F- 34095, Montpellier, France

ABSTRACT

Herein, we developed a precursor approach toward the design of a titanium nitride (TiN)/silicon nitride (Si_3N_4) nanocomposite with activated carbon monolith as a support matrix forming a highly micro-/mesoporous component to be used as a Pt support for the catalytic hydrolysis of sodium borohydride ($NaBH_4$) as a model reaction. The experimental data demonstrates that the amorphous Si_3N_4 matrix, the strong Pt-TiN nanocluster interaction and the synergistic effects between the three components contributed to the improved performance of the catalyst system. Thus, the use of this TiN/Si_3N_4 nanocomposite allowed to significantly reducing the noble metal loading (only ~1 wt% of Pt) for the complete and fast dehydrogenation of $NaBH_4$ under alkaline conditions at 80 °C. Additionally, the catalytic system displayed an excellent robustness and durability to offer reusability without collapsing and performance decrease under the harsh conditions imposed by the reaction.

1. Introduction

Discovery and identification of new materials is a key element of the innovation cycle of energy conversion, transmission and storage technologies and appears to be essential for driving technological energy development.[1] The effective usage of these energy systems is often associated with the design and development of new advanced catalysts with well-controlled nanostructure.[2] Such functional materials could provide an effective way to solve the problems concerning the processes of energy storage, conversion and utilization and have a positive economic as well as environmental impact, particularly in the area of clean energy technologies.

To highlight the challenge related to catalyst for energy, the global catalysis market is expected to reach $34.3 billion in 2024, according to a report by Grand View Research, Inc..[3]

This global challenge provides excellent opportunities for material experimentalists and theorists in the design and exploration of new materials as catalysts.[4]

The performance of a catalyst is closely related to the number of active sites, then it can be significantly improved through the modulation of the catalyst characteristics: i) composition, ii) morphology (*e.g.,* nanostructuration) and iii) architecture (*e.g.*, porous with control pore size at different length scales). However, identifying and creating a catalyst is complex, especially as the potential number of materials, defined by composition and particle size and shape, is overwhelming. Furthermore, one of the main obstacles on catalytic systems remains how to develop robust and durable catalysts, being present in a small proportion, in order to achieve long life span and reduced costs in energy systems.

Apart from the benchmark carbonaceous materials as catalyst supports and platinum (Pt) group metals (PGMs)-based catalysts, compounds that combine the properties of ceramic materials and transition metal (TM) such as TM oxides, carbides, nitrides, silicides and borides are emerging as environmentally benign alternatives and active materials for catalytic applications.[5-11] They not only show higher corrosion resistance than pristine TM and carbonaceous materials but also long-term stability at much lower costs. Each catalyst exhibits worthy advantages and disadvantages. Among solid-state compounds and materials, TM oxides (TMOs) are by far the most ubiquitous and extensively studied and characterized. As compared to TMOs, TM nitrides (TMNs) are also versatile compounds that formed with most of the periodic table components, especially many metals. TMNs, which have been introduced in the mid-21st century, belong to a class of materials that feature an unusual combination of outstanding properties, amongst which are their high melting points, exceptional hardness, high electrical conductivity and chemical stability such as high resistance against corrosion.[12]

Titanium nitride (TiN), as a typical representative of TMNs, has a metal-like conductivity with an outstanding chemical stability. TiN has been mainly investigated as a support of Pt because the modification of the electronic structure of Pt catalysts by interaction with TiN supports can significantly enhance the activity and durability of the catalyst.[13] Thus, Pt-supported TiN has been reported to exhibit higher performance and durability than commercial Pt-supported carbon due to strong metal-support interactions.[14-16] Therefore, TiN represent ideal alternatives to carbon materials across a wide range of catalytic reactions.

Designing TiN at nanoscale and developing micro-/mesoporous TiN with a large surface area that both provide selectivity and active sites to be effectively accessed for catalysis remain extremely challenging [17-27] while these are pre-requisite aspects to explore the full potential of TiN as an efficient and robust catalyst support or even as a co-catalyst.

To face these issues, we report the design of TiN/Si_3N_4 nanocomposite-based catalysts *via* a precursor route in which the nanocomposites consists of homogeneously distributed TiN nanoclusters in a robust and covalently bonded Si_3N_4 matrix. The nanocomposite, as a thin coating, has been supported on activated carbon monoliths to develop the micro-/mesoporosity of the support. Thus, we combine in the same materials both aspects, *i.e.*, micro-/mesoporosity and nanoscale synthesis, to be considered for heterogeneous catalysis and we exploited the potential of these functional materials as Pt supports to form a new efficient and robust catalyst system (Figure 1).

Figure 1

In the first part of this report, we used activated carbon monoliths as a support matrix of the functional TiN/Si_3N_4 nanocomposites to form a robust material bearing interconnected micro- and mesoporosity and very high specific surface areas. The characterization of the materials has

been done at various length scales. In the second part of the paper, the system has been exploited

to support a very low loading of Pt nanoparticles to be used as efficient and durable catalysts in

the hydrolysis sodium borohydride (NaBH$_4$) as a model reaction.

NaBH$_4$ has been declared by the US DOE as a no go source of hydrogen, but only for light

vehicle applications, because of low effective gravimetric hydrogen storage capacity (as all of

the materials investigated for hydrogen storage), and high cost with respect to recycling of its

hydrolysis borate by-product. It is still a candidate for other portable and mobile applications.

Quite a lot of effort has been put into developing catalyst systems for cheaper regeneration of

NaBH$_4$ from the borate by-product [28,29]. From the point of view of our work, NaBH$_4$ has been

used as a model system since it provides one of the harshest conditions during the hydrolysis

process in terms of temperature (80°C) and pH (14) among all potential sources of chemical

hydrogen storage. These conditions allowed us to demonstrate the effectiveness of our catalyst

system in terms of durability, reusability and cyclability. Under these conditions, some current

systems based on oxides of aluminum and silicon collapse due to structural failures in the

porosities and high leaching of active metal content. Carbon based systems under these

conditions face the issue of swelling which causes blockage of porosities and loss of

effectiveness. In other words, in our work, NaBH$_4$ is merely a model system, and does not aim at

comparing the hydrogen generation rates with previously reported catalysts [30-32].

Herein, our results evidence the performance of the TiN/Si$_3$N$_4$ nanocomposite-based catalyst

in comparison to mesoporous Si$_3$N$_4$, TiN-based catalysts as well as with catalysts derived from

activated carbon monoliths. The hydrolysis of NaBH$_4$ proceeds rapidly with 100 % H$_2$ release at

80 °C in an alkaline solution and the entitled materials demonstrated robustness and durability

for hydrogen generation from NaBH$_4$ after several cycles. The origin of the experimentally

observed enhanced catalytic activity and stability of the active Pt catalysts when dispersed on TiN/Si$_3$N$_4$ supports has been clarified by complementary techniques and greatly advance our knowledge-driven design of heterogeneous catalysts. This report provides first evidence that Pt/TiN support interactions as well as Si$_3$N$_4$ catalytic activity appear to play a pivotal role in the performance of catalytic systems to boost hydrogen release from hydrides. Thus, this work highlights the effectiveness and robustness of the TiN/Si$_3$N$_4$-based catalysts for the current effort toward an implementation of clean, affordable and renewable energy sources.

2. Experimental part

2.1. General Comments.

Synthesis reactions are performed under argon passing through successive columns of BTS-catalyst and P$_2$O$_5$ using standard Schlenk manipulations and vacuum/argon lines. Schlenk tubes are dried at 120°C overnight before pumping under vacuum and filling them with argon for synthesis. All chemical products are handled in an argon-filled glove box (Jacomex, Campus-type; O$_2$ and H$_2$O concentrations kept at < 0.1 ppm and 0.8 ppm, respectively). Toluene (99.85 %, Extra Dry over Molecular Sieve, AcroSeal(R)) is purchased from Acros Organics. Poly(perhydropolysilazane) (PHPS, AQUAMICA NN-310) was provided by Mitsuya Boeki Ltd., Japan. Anal. Found (wt%): Si, 65.1; N, 26.2; H, 8.3; O, 0.4. FTIR (KBr/cm^{-1}): ν(N−H) = 3374 (m), ν(Si−H) = 2125 (s), ν(N-H) = 1180 (s), ν(Si-N) = 840-1020 (s). ^{1}H NMR (500 MHz, C$_6$D$_6$, δ/ppm): 1.6-0.3 (NH), 5.8-4.3 (SiH). Activated Carbon monoliths labelled as AC were of type NORIT RX3 (Cabot Corporation) with a purity of 97% (SSA = 989 m^2.g^{-1}; Vp = 0.51 cm^3.g^{-1}; Øp = 4.3 nm). Chloroplatinic acid hexahydrate (H$_2$PtCl$_6$·6H$_2$O, Sigma-Aldrich), sodium borohydride (NaBH$_4$, Acros Organics), sodium hydroxide (NaOH, Carlo Erba) and deionized

ultra-pure water (Milli-Q grade; resistivity > 18 MΩ cm) are used to prepare the catalytic system and perform the catalytic reaction.

2.2. Preparation of micro-/mesoporous samples.

The synthesis of **PHTiPS2.5** has been performed according to our previous papers.[33-35] Anal. Found (wt%): Si, 30.9; N, 15.4; Ti, 19.2; C, 26.4; H, 6.2; O, 1.9. Then, **PHTiPS2.5** has been used to coat AC samples. The latter have been previously heat-treated at 600°C under vacuum (3.10^{-1} mbar) for 10 hours to remove presence of any trace of oxygen, moisture or dangling groups (-OH, -COOH, etc) without structure modification; then, they have been stored inside the glove box. A specific weight of AC was taken from the glove box in a Schlenk-type flask to be put under vacuum before deposition of the **PHTiPS2.5** sample in solution (5 wt%). AC samples are infiltrated at reduced pressure by the **PHTiPS2.5** sample according to an optimum mass ratio between the polymer and AC (1.4). Then, the composites were allowed to age for 24 h under static vacuum with continuous ultra-sonication. After aging for 24 h, a filtration step is performed and the composites were washed with toluene under argon flow. Excess of liquid is removed using a syringe and then the solvent is evaporated at low pressure (5.10^{-1} mbar) at 30°C for 2 h to generate the coated AC. The impregnated monoliths were dried and transferred under protective atmosphere into a horizontal tube furnace (Thermoconcept® OS50/450/12) to be subjected to a cycle of ramping at 100°C h^{-1} to 400°C under nitrogen, dwelling there for 2 h. This was followed by a pyrolysis under ammonia at 100°C h^{-1} to 1000°C, dwelling there for 5 h. Cooling to RT at 2°C min^{-1} produced **mSiTiN10** samples. For comparison, **mSi₃N₄** samples have been prepared using the same procedure. The **mSiTiN10** samples were then annealed in a graphitic furnace (Gero Model HTK 8) through a cycle of

ramping at 5°C min^{-1} to 1400°C, remaining there for 2 h and then cooling down to RT at 2°C min^{-1} generating **mSiTiN14** samples. For comparison, **mTiN14** samples have been prepared using the same procedure.

2.3. Preparation of Pt-supported micro-/mesoporous samples.

Platinum nanoparticles have been deposited on the different samples using wet impregnation process. A platinum salt (Chloroplatinic acid hexahydrate ($H_2PtCl_6 \cdot 6H_2O$)) is dissolved in excess of water and then agitated for 24 h with a specific quantity of the samples prepared in section 2.2. The samples are then dried in an oven to remove excess water and allow the platinum to be precipitated as nanoparticles in the porosities of the monolith. The precipitated platinum salts are then reduced under a flow of 5% H_2 in Ar at 450°C for 4 h.

2.4. Characterization

The Brunauer–Emmett–Teller (BET) method has been used to calculate the specific surface area of the samples. The pore-size distribution is derived from the desorption branches of the isotherms using the *Barrett–Joyner–Halenda* (BJH) method whereas the total pore volume is estimated from the amount of N_2 adsorbed at a relative pressure (P/P$_0$) of 0.97. The data are collected using a Micrometrics ASAP 2020 apparatus. ICP-MS (Silicon, titanium and platinum contents) and nitrogen, carbon, oxygen contents have been performed at the University of Montpellier (France) on the polymeric and ceramic samples. The specimens have been observed on a high resolution S4800-FEG SEM from Hitachi. A lower resolution SEM EVO HD 15 from Zeiss has been used to perform Energy Dispersive X-ray spectroscopy (EDXS) for point areas and for surface mapping of the elements present in the samples. A scanning transmission

electron microscope (STEM) has been performed on the samples using a FEI Titan 80-300 operating at an acceleration voltage of 300 kV. For the EELS acquisition, the convergence and collection semi angles have been approximately 3.6 and 13.7 mrad respectively. The dispersion has been set to 0.05 eV/channel and the Full Width at Half Maximum (FWHM) of the zero-loss peak has been 0.70 ± 0.05 eV. Samples have been crushed in isopropanol and a drop of solution has been placed onto a STEM grid (Agar Inc). The hydrolysis of $NaBH_4$ has been performed at 80°C in a highly alkaline medium (pH > 10). In a typical experiment, 16 mg of the Pt-supported nanocomposites are introduced in 1 ml solution of $NaBH_4$ (120 mg in 2% NaOH) into a reactor (glass tube) that is sealed with a silicon septum and Parafilm®, and connected to a water-filled inverted burette (water coloured in blue) via a cold trap for steam, maintained at 0°C. Then, the reactor is immersed in an oil bath kept at 80°C. A camera records the water displacement in the inverted burette due to hydrogen generation. Hydrogen starts to evolve rapidly and the evolution is video-recorded for 170-180 min, to be then computationally analysed post-hydrolysis. FT-IR spectra are recorded on as-prepared **mSi_3N_4** and water-treated **mSi_3N_4** with a JASCO FT/IR 4200 spectrometer at a resolution of 4 cm^{-1}. The water-treatment of sample was performed by immersing the sample within distilled water at room temperature (R.T.) for 12h. Prior to the measurement, sample was diluted to 5wt% by potassium bromide (KBr). Self-standing sample disk was prepared by pressing the mixed powder sample. The disk is placed in an IR cell with CaF_2 window. After recording of initial IR data at R.T., 10 Torr of pyridine are introduced to the IR cell. Then, IR spectra for the pyridine adsorbed sample was recorded after evacuation at specific temperatures (R.T., 40 ºC, 100 ºC, 150 ºC and 200 ºC). Diffuse reflectance infrared Fourier transform spectroscopy (DRIFTS) analyses were carried out to clarify the difference of the surface nature between wet- **mSi_3N_4** and wet-**SiTiN14** with a FT-IR spectrometer (Model

spectrum TM100, Perkin Elmer Japan Co., Ltd., Tokyo, Japan) at a resolution of 4 cm^{-1}. Prior to the measurement, sample is treated under flowing high purity Ar at 50°C for 30 min.

3. Results and discussion

NaBH$_4$ displays a high stability in solid state does not display safety issues (*e.g.*, volatility, toxicity, corrosivity, *etc.*) for practical use. In water, molecular hydrogen is released by reaction of one hydridic hydrogen (H$^{\delta-}$) of NaBH$_4$ with one protic hydrogen (H$^{\delta+}$) of H$_2$O. However, the self-hydrolysis of NaBH$_4$ is slow at room temperature, which makes the use of suitable catalysts required to achieve hydrogen release at appreciable rates. Platinum(0) is among the catalysts with the highest activity in hydrolysis of NaBH$_4$.[36,37] Therefore, the catalytic hydrolysis of NaBH$_4$ induces the release 4 equiv. H$_2$ (Eq. 1) without gaseous contamination (*e.g.*, ammonia) in contrast to other types of boron-based chemical hydrogen storage materials such as ammonia or hydrazine borane.[38]

$$NaBH_4(aq) + (2 + x)H_2O(l) \xrightarrow{catalyst} NaBO_2 . xH_2O(aq) + 4H_2(g) \qquad (1)$$
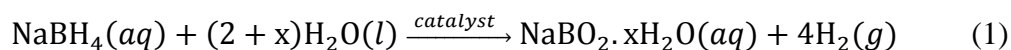
The reaction is exothermic (ΔH, *ca*. -250 kJ/mol) and the by-product sodium tetrahydroxyborate is a strong base (pKa = 9.3) which significantly increases the pH of the solution (pH > 10). Thus, the widely-used oxide and carbonaceous supports suffer from serious drawbacks under the reaction conditions: shortened lifetime for oxide supports because of degradation and swelling of carbonaceous supports blocking the pore access.[36] Another difficulty faced by these systems is the leaching of the active metal nanoparticles due to weak metal-support interactions causing tremendous loss in catalytic activity.[39,40] Thus, the catalytic hydrolysis of NaBH$_4$ has been selected as a model reaction in our work in order to

evaluate the potential of TiN/Si$_3$N$_4$ nanocomposite-based catalysts in terms of effectiveness, robustness and durability.

3.1. Preparation of micro-/mesoporous samples

Our route consisted to coat activated carbon monoliths (AC) with a preceramic polymer (**PHTiPS2.5**; Si$_{1.0}$Ti$_{0.4}$C$_{2.0}$N$_{1.0}$H$_{5.6}$, neglected oxygen content because < 2wt% [33-35]) to macroscopically shape the monolithic-type structure of the support. AC is used as a support matrix also to overcome the problems related to the poor mechanical stability of polymer-derived ceramics with highly developed mesoporosity.[41-42] The synthesis of the polymer has been directed to provide polymer processability in solution and lead, after pyrolysis under ammonia then annealing under nitrogen, to TiN/Si$_3$N$_4$ nanocomposites.[33-35] Impregnation of AC (and solvent evaporation) was followed by a two-step pyrolysis under nitrogen (400 °C) to crosslink the polymer surrounding AC samples, then under ammonia (1000 °C) to form the **mSiTiN10** sample (composition of the ceramic coating is Si$_{1.0}$Ti$_{0.5}$N$_{2.0}$O$_{0.2}$ (the carbon content is 0.05 wt%, therefore omitted)). A final annealing step under nitrogen (1400 °C) allowed forming the **mSiTiN14** sample (composition of the ceramic coating is Si$_{1.0}$Ti$_{0.5}$N$_{1.8}$ (neglected carbon and oxygen contents with 0.003 and 1.23 wt%, respectively)).

As expected, as-obtained materials reproduce the monolithic shape of AC samples (Figure 1 as insert). The **mSiTiN10** (*Figure 1SI in ESI*) and **mSiTiN14** (Figure 2) samples have been characterized by nitrogen sorption measurements at 77 K.

Figure 2

The analysis of the nitrogen sorption isotherms by the Brunauer-Emmett-Teller (BET) method reveals that both samples have similar complex isotherms composed of types II and IV.[43] The

fast increase of adsorption at low P/P_0 reflects the presence of micropores. The distinct hysteresis loop between the adsorption and desorption (P/P_0 from 0.4 to 1.0), identifiable as a H2-type [43] demonstrates the presence of mesopores generally found in disordered porous materials with 3-D cage-like pores and pore interconnectivity.[44] Based on the structure of AC [41], samples can be considered as disordered micro-/mesoporous materials bearing interconnected porosity. The BET specific surface area (SSA), *i.e.*, 1345 $m^2.g^{-1}$ (**mSiTiN10**) and 1217 $m^2.g^{-1}$ (**mSiTiN14**), are significantly high and the Barrett-Joyner-Halenda (BJH) analysis (Figure 2 as insert) suggests a narrow pore size distribution of 3.3 nm (**mSiTiN10**) and 3.4 nm (**mSiTiN14**). Total pore volumes of 0.72 $cm^3.g^{-1}$ (**mSiTiN10**) and 0.67 (**mSiTiN14**) $cm^3.g^{-1}$ are measured and a typical t-Plot micropore volume of 0.42 $cm^3.g^{-1}$ is measured for both samples. The very high SSA values tends to confirm that AC is still present in the materials as expected. To confirm the presence of the carbon template as a support matrix of nanocomposites, we investigated Raman spectroscopy of the **mSiTiN14** sample. The Raman spectrum of **mSiTiN14** exhibits two absorptions at 1350 and 1580 cm^{-1} assigned to the D and G bands of carbon whereas the spectrum of the nanocomposite powder analogue shows an absorption band at 480 cm^{-1} characteristics of the face-centered cubic (fcc) TiN phase [34] without peaks characteristic of carbon (*Figure 2SI in ESI*). This clearly confirms the presence of AC as a support matrix. The XRD patterns of **mSiTiN10** and **mSiTiN14** samples (*Figure 3SI in ESI*) reveal that crystallization of the face-centered cubic (fcc) TiN phase gradually takes place with increasing the temperature of pyrolysis from 1000 °C (**mSiTiN10** sample) to 1400 °C (**mSiTiN14** sample). TiN is better identified in the **mSiTiN14** sample by the presence of peaks at $2\theta = 36.7°$, $42.7°$, $62.1°$, $74.4°$ and $77.9°$, which are attributed to the (111), (200), (220), (311) and (222) fcc TiN reflections and no further XRD peaks are observed. Based on the ceramic formula of the **mSiTiN14** sample ($Si_{1.0}Ti_{0.5}N_{1.8}$), we

can confirm the formation of Si_3N_4; the latter displaying an amorphous structure. Because the **mSiTiN10** sample is poorly crystallized with very broad TiN XRD peaks, only the **mSiTiN14** sample has been further studied by HAADF-STEM (Figures 3-4). The low magnification HAADF-STEM images (Figure 3) of the **mSiTiN14** sample shows the presence of nanoscaled precipitates embedded in a network with the typical phase contrast of an amorphous matrix, Si_3N_4. This confirms the formation of a nanocomposite-type structure in the **mSiTiN14** sample.

Figure 3

Figure 4a shows the overlap of highly faceted nanocrystals with a lattice spacing of 0.24 ± 0.02 nm corresponding to the (111) planes of the fcc TiN phase (Figure 4b). Based on the Fast Fourier Transform (FFT) data collected from the highlighted enclosed area in the inset of Figure 4b, the indexing of fcc TiN has been also confirmed. The peak identified in the EELS spectrum at 456 eV *(Figure 4SI in ESI)*, after the background subtraction, is attributed to the Ti $L_{2.3}$ edge.

Figure 4

By combining elemental analyses and nitrogen sorption measurements with results derived from Raman spectroscopy, X-Ray diffraction and HAADF-STEM investigations, we confirm that the investigated samples represent materials bearing interconnected micro-/mesopores made of carbon supporting a poorly crystallized ceramic coating (**mSiTiN10**) or a nanocomposite (**mSiTiN14**) coating made of TiN nanoclusters homogeneously distributed in a Si_3N_4 amorphous matrix.

3.2. Preparation of Pt-supported micro-/mesoporous samples

After deposition of Pt nanoparticles, as-obtained samples, denoted as **Pt/mSiTiN10** and **Pt/mSiTiN14**, are investigated through nitrogen sorption measurements (*Figure 5SI* (**Pt/mSiTiN10**) and Figure 5 (**Pt/mSiTiN14**)). The BET isotherms of **Pt/mSiTiN10** and

Pt/mSiTiN14 are similar to those of Pt-free samples with comparable SSA, *i.e.*, 1098 $m^2.g^{-1}$ (**Pt/mSiTiN10**) and 1307 $m^2.g^{-1}$ (**Pt/mSiTiN14**). This is related to the very low amount of Pt precursor which is deposited on the support. Our target was indeed to deposit only 1 wt% (< 0.2 mg) of Pt to highlight the attractivity of the support for catalysis-assisted reactions.

Figure 5

The **Pt/mSiTiN14** sample has been studied by HAADF-STEM (Figures 6a-b and *Figure 6SI*), EELS (Figure 6c) and ICP to confirm the presence of Pt and the morphology, size and content of nanoparticles. The low magnification HAADF-STEM (Figure 6a) and BF-STEM (*Figure 6SI in ESI*) images of the **Pt/mSiTiN14** sample nicely reflect the nanostructure of the samples made of TiN and Pt platelets (6-8 nm in diameter) and an amorphous matrix. It confirms the high distribution of nanoscaled precipitates, *i.e.*, TiN and Pt, in/on the matrix. The Pt content is found to be 0.91 wt% (0.14 mg) by ICP. For comparison, the Pt content of the **Pt/mSiTiN10** sample has been determined to be 1.07 wt% (0.17 mg). The EELS analyses confirm the presence of Pt in the **Pt/mSiTiN14** sample as exemplified by the spectrum (Figure 6c) extracted from the high magnification STEM image in Figure 6b. Pt is characterized by the two prominent peaks centred at 2100 eV and 2750 eV assigned to the $M_{4.5}$ and M_3 edges of Pt, respectively.

Figure 6

As-characterized samples have been then tested during the hydrolysis of $NaBH_4$.

3.3. Catalytic activity of Pt-supported micro-/mesoporous samples

The catalytic performance of **Pt/mSiTiN10** and **Pt/mSiTiN14** (16 mg each) toward the dehydrogenation of 1.0 M $NaBH_4$ has been evaluated in a typical water-filled graduated burette

system in alkaline solution (pH > 10; 2% NaOH) at 80°C. Then, we measured the volume of hydrogen generated during 170-180 min of reaction (Figure 7).

Figure 7

The performance of these samples was then compared with that of Pt-supported mesoporous TiN and mesoporous Si_3N_4 labelled as **Pt/mTiN14** (1.26 wt% Pt (or 0.2 mg), as measured by ICP) and **Pt/mSi₃N₄** (1.12 wt% Pt (or 0.18 mg)) prepared according to the same procedure of **Pt/mSiTiN14** and **Pt/mSiTiN10** samples, respectively. The preparation and characterization of the **mSi₃N₄** sample is done according to the procedure applied to prepare the **mSiTiN10** sample. Note that the Si_3N_4 support was prepared at 1000 °C to keep the Si_3N_4 phase amorphous.[41] It displays SSA values of 653.8 m^2 g^{-1} before Pt deposition and 357.7 m^2 g^{-1} after Pt deposition.[41] Concerning the mesoporous TiN (*Figure 7SI in ESI*), the sample was prepared according to the procedure to prepare the **mSiTiN14** sample. It displays the characteristic XRD peaks of fcc-TiN and shows types II and IV isotherms with a H_2 hysteresis loop and SSA values of 900.3 m^2 g^{-1} before Pt deposition and 872 m^2 g^{-1} after Pt deposition, respectively. Although the samples display different textural properties, Figure 7 shows that there is a clear tendency in the plots of H_2 evolution versus time for the hydrolysis of $NaBH_4$. The **Pt/mSiTiN14** sample exhibits the highest activity among all the catalysts prepared in this work: The rate of hydrogen generation (slope of the curves at a conversion < 50%) normalized to per gram of platinum is 39 $L.min^{-1}.g_{pt}^{-1}$ (**Pt/mSiTiN14**) to be compared with 24.2 (**Pt/mSi₃N₄**), 14.9 (**Pt/mSiTiN10**), and 5.6 (**Pt/mTiN14**) $L.min^{-1}.g_{pt}^{-1}$. Beside this, the **Pt/mSiTiN14** sample showed a significantly higher performance than Pt/AC samples (AC being the support used to deposit the nanocomposites; Pt has been deposited according to a same procedure) (*Figure 8SI in ESI*). This clearly highlights that the nanocomposite coating significantly enhances the catalytic activity of

AC samples. Only the **Pt/mSiTiN14** sample provides the complete dehydrogenation of $NaBH_4$, *i.e.* the release of 4 equiv. H_2 after 90 min of reaction. The other catalysts are deactivated before the completion of hydrolysis. First, it can be suggested that the precipitation of TiN nanoclusters in an amorphous Si_3N_4 matrix, *i.e.*, the **mSiTiN14** sample, contributes to the highest performance of the derived catalyst compared to the catalysts derived from the poorly crystallized **mSiTiN10** and amorphous **mSi₃N₄** supports. This highlights Pt-support interactions in the **Pt/mSiTiN14** sample, most probably between TiN nanoclusters and Pt nanoparticles. At the opposite, the **Pt/mTiN14** sample displays the lowest performance although the TiN phase is crystallized. We explain this result by the fact that TiN is not nanoscaled in **mTiN14** as in the nanocomposite system, *i.e.*, the **mSiTiN14** sample. In the latter, the covalently-bonded Si_3N_4 matrix retain the nanosize of the TiN clusters. Thus, TiN, if alone and/or not nanoscaled, cannot meet the requirements as a suitable catalytic support for Pt in the hydrolysis of $NaBH_4$. Interestingly, the **Pt/mSi₃N₄** sample provides a higher catalytic activity in the hydrolysis of $NaBH_4$ than the **Pt/TiN14** sample. In order to highlight the role of both the TiN nanoclusters and the amorphous Si_3N_4 matrix in the performance of the catalyst system, we explored the catalytic activity of the supports tested in Figure 7 (except the **mSiTiN10** sample) without deposition of Pt.

3.4. Role of TiN nanoclusters and amorphous Si₃N₄ in the performance of the catalyst system.

   Figure 8 shows the plots of H_2 evolution versus time for the hydrolysis of $NaBH_4$ using the **mSiTiN14**, **mTiN14** and **mSi₃N₄** samples. As expected, the absence of Pt affects the catalytic activity of all the samples; in particular, for the **mSiTiN14** support. This definitively confirms the synergy between Pt and TiN nanoclusters. In addition, it is very surprising to identify a relatively high catalytic activity for the **mSi₃N₄** sample in the hydrolysis of $NaBH_4$. This tends to

demonstrate that amorphous Si_3N_4 plays a key role in the performance of the TiN/Si_3N_4 nanocomposite-based catalyst, *i.e.*, the **mSiTiN14** sample. To the best of our knowledge, this is the first report that metal-free polymer-derived ceramics (PDCs) are found to be catalytically active whereas only two studies report the use of porous silicon nitride materials as basic catalysts.[17,18,45]

To understand the role of TiN nanoclusters and amorphous Si_3N_4 matrix in the catalytic activity of the system, we investigated the surface acido-basic centers of the **mSi$_3$N$_4$** sample by FT-IR spectroscopy (Figure 9) based on the observation of the vibrational perturbation undergone by pyridine when it adsorbs on it. Pyridine is the most largely used basic probe molecule for surface acidity characterization.[46-48] Thus, the shift of the position of some very sensitive bands of the adsorbate upon adsorption in the FT-IR spectrum can be taken as a measure of the Lewis acid strength of the surface sites in the **mSi$_3$N$_4$** sample.

Figure 9

As shown in Figure 9(a), as-synthesized **mSi$_3$N$_4$** exhibited absorption bands as a basic catalyst at 3380, 3180 and 1400 cm^{-1} assigned to Si-NH-Si, $Si-NH_3^+$ and $=NCOO^-$ (formed situ between the surface NH and CO_2 in atmosphere), respectively. However, under the hydrolysis condition fixed in the present study, surface Si-OH groups formed *in-situ* on the **mSi$_3$N$_4$** acted as water adsorption site *via* hydrogen bond to afford polar OH groups. (Figure 9(b)).

Actually, after pyridine adsorption to **mSi$_3$N$_4$**, this acid site was clearly detected as typical adsorption bands at 1594 and 1445 cm^{-1} attributed to hydrogen-bonded pyridine (Py-H) [49] which was easily removed by heating to 200 ℃ under vacuum (Figure 10). Moreover, the surface Si-OH was also detected for the **mSi$_3$N$_4$** after the water treatment followed by drying at 50 ℃ under Ar flow (*Figure 9SI in ESI*).

Figure 10

Interestingly, the **mSiTiN14** sample exhibits a very low content of surface hydroxyl group compared to the **mSi$_3$N$_4$** sample after water treatment. Thus, the results indicate that TiN nanoclusters improve the stability of Si$_3$N$_4$ toward hydrolysis of support while reducing the catalytic property of the nanocomposite for the generation of protonic hydrogen.

Based on the results shown above, the enhanced H$_2$ generation achieved for the TiN/Si$_3$N$_4$ nanocomposite-based catalyst, *i.e.*, **Pt/mSiTiN14** sample, is explained by the synergistic effect shown in Figure 11.

Figure 11

During NaBH$_4$ hydrolysis (Eq. 1), hydridic hydrogen (H$^{\delta-}$) are efficiently produced by the Pt-TiN electron conductive nanoclusters. On the other hand, the coordination of ions at the "ideal" surface is necessarily uncomplete with respect to the coordination in the bulk. Thus, in our experiments, the 'semi-metal' (Si) cations, acting as an acid site according to the Lewis definition, are expected to react with species from the environment such as water, to decrease the free energy of the atoms exposed at the surface of the material. Water saturates the coordinative unsaturations, so that in this case Lewis acidity are expected to completely disappear while surface hydroxy-groups are formed, potentially responsible for Brønsted acidity (*See Figure 10SI in ESI*). The formation of protonic hydrogen (counterpart for the H$_2$ generation) from water molecule is thought to be catalyzed by the acid site formed *in-situ* on the Si$_3$N$_4$ matrix. It should be noted that the proper nanocomposite structure of electron conductive TiN nanoclusters embedded within electron insulating mesoporous amorphous Si$_3$N$_4$ is important to afford hydridic hydrogen efficiently since the monolithic electron conductive TiN matrix only acted as an electron acceptor, which could lead to the lower catalytic activity observed for the

Pt/mTiN14 sample. On the other hand, in the case of the **mSiTiN10** sample the size of TiN nanoclusters was too small to provide "triple junction" of BH_4^--Pt-TiN or low crystallinity to offer sufficient electron conduction.

3.5. Recyclability tests

   The recycle stability is of crucial importance to the practical application of catalysts; thus, the durability tests of Pt-supported micro-/mesoporous samples were carried out 5 times. As shown in Figure 12, the **Pt/mSiTiN14** sample does not show any signs of degradation in terms of catalytic activity even after 5 recyclability tests. The release of H_2 remains unchanged and the structural integrity is retained according to the fact that the BET isotherm still remains a mix of types II and IV with a H2 hysteresis (*See Figure 11SI in ESI*) and a SSA value of 1248 $m^2.g^{-1}$ is calculated. This clearly indicates that the catalytic system has long durability most probably because of the presence of Si_3N_4 as a matrix preventing TiN nanocluster growth and protecting TiN nanocrystals against corrosion. This also showed that AC, as a support matrix, overcomes the problems related to the poor robustness of polymer-derived ceramics with highly developed mesoporosity. Furthermore, retaining the initial catalytic activity after five tests of $NaBH_4$ hydrolysis suggests that there is no detectible leaching of Pt nanoparticles from the surface of nanocomposite support into the solution during the reaction.

Figure 12

   The Pt content on the support after 5 cycles of hydrolysis is determined by ICP to be 0.92 wt%. This proves that the nanocomposite coating effectively immobilizes Pt nanoparticles. There is an increase of 1.5% in B content on the support tested after the 5th cycle suggesting the

presence of crystallizing borates on the surface of the monoliths, which does not affect properties.

4. Conclusions

In summary, we have synthesized robust and highly micro-/mesoporous monoliths made of an amorphous Si_3N_4 coating with integrated TiN nanocrystallites surrounding an activated carbon monolith. As-prepared samples displayed BET SSA close to 1300 $m^2.g^{-1}$ and could support highly dispersed Pt nanoparticles. The particular structural organization and composition of the nanocomposite coatings, i.e., growth of TiN at nanoscale directly in the Si_3N_4 matrix, allowed to significantly reduced the quantity of Pt (around 1 wt%) required in the derived catalytic system for the complete dehydrogenation of sodium borohydride ($NaBH_4$). TiN nanocrystals provided synergy with the Pt nanoparticles deposited on the nanocomposite whereas the covalently-bonded Si_3N_4 offered catalytic activity, avoided sintering of the TiN nanocrystals and corrosion in the conditions we imposed to produce hydrogen from $NaBH_4$. It results a robust catalytic system (because of the presence of AC as a support matrix), reusable, with outstanding hydrogen production performance (100 % H_2 release) and excellent stability in an alkaline medium at 80°C for the complete hydrolysis of $NaBH_4$, even after 5 successive runs. To highlight the benefit of these nanocomposites, we compared their performance with those of mesoporous Si_3N_4 and TiN as well as activated carbon. This study paves the way for the rational synthesis of robust nitride nanocomposite-based catalysts that may be applied in a wide range of catalysis-assisted reactions for energy-related fields.

References

[1] D. Gielen, F. Boschell, D. Saygin, Climate and energy challenges for materials science, Nature Mater., 15 (2016) 117-120. https://doi.org/10.1038/nmat4545.

[2] S. L. Suib, (Ed) New and future developments in catalysis, (Ed: S. L. Suib), Elsevier, 2013.

[3] Catalyst Market Analysis By Raw Material, By Product, Application And Segment Forecasts To 2024, Grand View Research, Inc, June 2016.

[4] L. Huang, P.-C. Chen, M. Liu, X. Fu, P. Gordiichuk, Y. Yu, C. Wolverton, Y. Kang, C. A. Mirkin, Catalyst design by scanning probe block copolymer lithography, Proc. Natl. Acad. Sci. U.S.A, 115 (2018) 3764-3769. https://doi.org/10.1073/pnas.1800884115.

[5] E. Y. Choi, C. K. Kim, Fabrication of nitrogen-doped nano-onions and their electrocatalytic activity toward the oxygen reduction reaction, Sci. Rep., 7 (2017) 4178. https://doi.org/10.1038/s41598-017-04597-6.

[6] J. C. Védrine, Heterogeneous Catalysis on Metal Oxides, catalysts, 7 (2017) 341-365. https://doi.org/10.3390/catal7110341

[7] Y. Zhong, X. Xia, F. Shi, J. Zhan, J. Tu, H. J. Fan, Transition Metal Carbides and Nitrides in Energy Storage and Conversion, Adv. Sci., 3 (2016) 1500286-1500313. https://doi.org/10.1002/advs.201500286

[8] J. S. J. Hargreaves, Heterogeneous catalysis with metal nitrides, Coord. Chem. Rev., 257 (2013) 2015-2031. https://doi.org/10.1016/j.ccr.2012.10.005.

[9] M.-S. Balogun, Y. Huang, W. Qiu, H. Yang, H. Ji, Y. Tong, Updates on the development of nanostructured transition metal nitrides for electrochemical energy storage and water splitting, Mater. Today, 20 (2017) 425-451. https://doi.org/10.1016/j.mattod.2017.03.019

[10] G. Mera, M. Gallei, S. Bernard, E. Ionescu, Ceramic Nanocomposites from Tailor-Made Preceramic Polymers, Nanocomposites 5 (2015) 468-540. https://doi.org/10.3390/nano5020468.

[11] S. Klemenz, J. Schuch, S. Hawel, A. M. Zieschang, B. Kaiser, W. Jaegermann, B. Albert, Synthesis of a Highly Efficient Oxygen-Evolution Electrocatalyst by Incorporation of Iron into Nanoscale Cobalt Borides, ChemSusChem 11 (2018) 3150-3156. https://doi.org/10.1002/cssc.201801547

[12] S. T Oyama, The Chemistry of Transition Metal Carbides and Nitrides, (Ed: S. T. Oyama), Springer, Berlin, Germany, 1996.

[13] H. Nan, D. Dang, X. L. Tian, Structural engineering of robust titanium nitride as effective platinum support for the oxygen reduction reaction, J. Mater. Chem. A. 6 (2018) 6065-6073. https://doi.org/10.1039/C8TA00326B.

[14] Y. Han, X. Yue, Y. Jin, X. Huang, P. K. Shen, Hydrogen evolution reaction in acidic media on single-crystalline titanium nitride nanowires as an efficient non-noble metal electrocatalyst, J. Mater. Chem. A. 4 (2016) 3673-3766. https://doi.org/10.1039/C5TA09976E.

[15] Z. Cui, M. Yang, F. J. DiSalvo, Mesoporous Ti(0.5)Cr(0.5)N supported PdAg nanoalloy as highly active and stable catalysts for the electro-oxidation of formic acid and methanol, ACS Nano 8 (2014) 6106-6113. https://doi.org/10.1021/nn5014337

[16] M. Yang, Z. Cui, F. J. DiSalvo, Mesoporous titanium nitride supported Pt nanoparticlesas high performance catalysts for methanol electrooxidation, Phys. Chem. Chem. Phys. 15 (2013) 1088-1092. https://doi.org/10.1039/C2CP44215A

[17] B. Qi, X. Zhao, S. Wang, K. Chen, Y. Wei, G. Chen, Y. Wei, G. Chen, Y. Gao, D. Zhang, Z. Sun, F. Li, Mesoporous TiN microspheres as an efficient polysulfide barrier for lithium–sulfur batteries, J. Mater. Chem. A, 6 (2018) 14359-14366. https://doi.org/10.1039/C8TA04920C.

[18] S. Kaskel, K. Schlichte, T. Kratzke, Catalytic Properties of High Surface Area Titanium Nitride Materials, Mol. Catal., 208 (2004) 291-298. https://doi.org/10.1016/S1381-1169(03)00545-4.

[19] S. Dong, X. Chen, L. Gu, X. Zhou, H. Xu, H. Wang, Z. Liu, P. Han, J. Yao, L. Wang, G. Cui, L. Chen, Facile Preparation of Mesoporous Titanium Nitride Microspheres for Electrochemical Energy Storage, ACS Appl. Mater. Interfaces, 3 (2011) 93-98. https://doi.org/10.1021/am100951h.

[20] J. H. Bang, K. S. Suslick, Dual Templating Synthesis of Mesoporous Titanium Nitride Microspheres, Adv. Mater., 21 (2009) 1-5. https://doi.org/10.1002/adma.200802309.

[21] N. Fechler, T.-P. Fellinger, M. Antonietti, Template-Free One-Pot Synthesis of Porous Binary and Ternary Metal Nitride@N-Doped Carbon Composites from Ionic Liquids, Chem. Mater., 24 (2012) 713-719. https://doi.org/10.1021/cm203667g.

[22] Z. Pan, Y. Xiao, Z. Fu, G. Zhan, S. Wu, C. Xiao, G. Hu, Z. Wei, Hollow and porous titanium nitride nanotubes as high-performance catalyst supports for oxygen reduction reaction, J. Mater. Chem. A, 2 (2014) 13966-13975. https://doi.org/10.1039/C4TA02402H.

[23] E. Ramasamy, C. Jo, A. Anthonysamy, I. Jeong, J. K. Kim, J. Lee, Soft-Template Simple Synthesis of Ordered Mesoporous Titanium Nitride-Carbon Nanocomposite for High Performance Dye-Sensitized Solar Cell Counter Electrodes, Chem. Mater., 24 (2012) 1575-1582. https://doi.org/10.1021/cm203672g.

[24] Y.-S. Jun, W. H. Hong, M. Antonietti, A. Thomas, Mesoporous, 2D Hexagonal Carbon Nitride and Titanium Nitride/Carbon Composites, Adv. Mater., 21 (2009) 4270-4274. https://doi.org/10.1002/adma.200803500.

[25] D.-R. Deng, T.-H. An, Y.-J. Li, Q.-H. Wu, M.-S. Zheng, Q.-F. Dong, Hollow porous titanium nitride tubes as a cathode electrode for extremely stable Li–S batteries, J. Mater. Chem. A, 4 (2016) 16184-16190. https://doi.org/10.1039/C6TA07221F.

[26] B. G. Kim, C. Jo, J. Shin, Y. Mun, J. Lee, J. W. Choi, Ordered Mesoporous Titanium Nitride as a Promising Carbon-Free Cathode for Aprotic Lithium-Oxygen Batteries, ACS Nano, 11 (2017) 1736-1746. https://doi.org/10.1021/acsnano.6b07635.

[27] Y.-M. Chi, M. Mishra, T.-K. Chin, W.-S. Liu, T.-P. Perng, ACS Appl. Mater. Interfaces. (2019)-Just accepted manuscript. https://doi.org/10.1021/acsaem.8b01426.

[28] L. Ouyang, W. Chen, J. Liu, M. Felderhoff, H. Wang, M. Zhu, Enhancing the Regeneration Process of Consumed NaBH4 for Hydrogen Storage, Adv. Energy Mater. 7 (2017) 1700299. https://doi.org/10.1002/aenm.201700299

[29] H. Zhong, L. Ouyang, M. Zeng, J. Liu, H. Wang, H. Shao, M. Felderhoff, M. Zhu, Realizing facile regeneration of spent NaBH4 with Mg–Al alloy, J. Mater. Chem. A, 7 (2019) 10723-10728. https://doi.org/10.1039/C9TA00769E

[30] P. Brack, S. E. Dann, K. G. U. Wijayantha, Heterogeneous and homogenous catalysts for hydrogengeneration by hydrolysis of aqueous sodium borohydride($NaBH_4$) solutions, Energy Science and Engineering, 3 (2015), 174–188, https://doi.org/10.1002/ese3.67

[31] A. Uzundurukan, Y. Devrim, Hydrogen generation from sodium borohydride hydrolysis by multi-walled carbon nanotube supported platinum catalyst: A kinetic study, Int. J. Hydrog. Energy, 44 (2019) 17586-17594, https://doi.org/10.1016/j.ijhydene.2019.04.188

[32] J. Guo, B. Wang, D. Yang, Z. Wan, P. Yan, J. Tian, T. T. Isimjan, X. Yang, Rugae-like Ni_2P-CoP nanoarrays as a bi-functional catalyst for hydrogen generation: $NaBH_4$ hydrolysis and water reduction, Appl. Catal. B 265 (2020) 118584,https://doi.org/10.1016/j.apcatb.2019.118584

[33] M. C. Bechelany, V. Proust, A. Lale, P. Miele, S. Malo, C. Gervais, S. Bernard, Nanocomposites through the Chemistry of Single-Source Precursors: Understanding the Role of Chemistry behind the Design of Monolith-Type Nanostructured Titanium Nitride/Silicon Nitride, Chem. Eur. J. 23 (2017) 832-845. https://doi.org/10.1002/chem.201603661.

[34] A. Lale, V. Proust, M. C. Bechelany, A. Viard, S. Malo, S. Bernard, A comprehensive study on the influence of the polyorganosilazane chemistry and material shape on the high temperature behavior of titanium nitride/silicon nitride nanocomposites, J. Eur. Ceram. Soc., 37 (2017) 5167-5175. https://doi.org/10.1016/j.jeurceramsoc.2017.04.001.

[35] M.-C. Bechelany, V. Proust, C. Gervais, R. Ghisleny, S. Bernard, P. Miele, In Situ Controlled Growth of Titanium Nitride in Amorphous Silicon Nitride: A General Route Toward Bulk Nitride Nanocomposites with Very High Hardness, Adv. Mater. 26 (2014) 6548-6553. https://doi.org/10.1002/adma.201402356.

[36] H. Zhang, X. Gu, P. Liu, J. Song, J. Cheng, H. Su, Highly efficient visible-light-driven catalytic hydrogen evolution from ammonia borane using non-precious metal nanoparticles supported by graphitic carbon nitride, J. Mater. Chem. A 5 (2017) 2288-2296. https://doi.org/10.1039/C6TA08987A.

[37] L. Ouyang, H. Zhong, H.-W. Li, M. Zhu, A Recycling Hydrogen Supply System of $NaBH_4$ Based on a Facile Regeneration Process: A Review, Inorganics, 6 (2018) 10-21. https://doi.org/10.3390/inorganics6010010.

[38] S. Ozkar, M. Zahmakiran, Hydrogen generation from hydrolysis of sodium borohydride using Ru(0) nanoclusters as catalyst, J. Alloys Compd. 404-406 (2005) 728-731. http://dx.doi.org/10.1016/j.jallcom.2004.10.084.

[39] H. Zhong, L. Ouyang, J. Liu ; C. Peng, X. Zhu, W. Zhu, F. Fang, M. Zhu, Sodium borohydride regeneration via direct hydrogen transformation of sodium metaborate tetrahydrate, J. Power Sources 390 (2018) 71-77. https://doi.org/10.1016/j.jpowsour.2018.04.037.

[40] M. Rivarolo, O. Improta, L. Magistri, M. Panizza, A. Barbucci, Thermo-economic analysis of a hydrogen production system by sodium borohydride ($NaBH_4$), Int. J. Hydrogen Energy 43 (2018) 1606-1614. https://doi.org/10.1016/j.ijhydene.2017.11.079.

[41] A. Lale, A. Wasan, R. Kumar, P. Miele, U. B. Demirci, S. Bernard, Organosilicon polymer-derived mesoporous 3D silicon carbide, carbonitride and nitride structures as platinum supports

for hydrogen generation by hydrolysis of sodium borohydride, Inter. J. Hydrogen Energy 41 (2016) 15477-15488. https://doi.org/10.1016/j.ijhydene.2016.06.186.

[42] C. Salameh, G. Moussa, A. Bruma, G. Fantozzi, S. Malo, P. Miele, U. B. Demirci, S. Bernard, Robust 3D Boron Nitride Nanoscaffolds for Remarkable Hydrogen Storage Capacity from Ammonia Borane, Energy Technol. 6 (2018) 570-577.

https://doi.org/10.1002/ente.201700618.

[43] M. Thommes, K. Kaneko, A. V. Neimark, J. P. Olivier, F. Rodriguez-Reinoso, J. Rouquerol, K. S. W. Sing, Physisorption of Gases, with Special Reference to the Evaluation of Surface Area and Pore Size Distribution, Pure Appl. Chem. 87 (2015) 1051-1069.

https://doi.org/10.1515/pac-2014-1117.

[44] G. Masson, The effect of pore space connectivity on the hysteresis of capillary condensation in adsorption—desorption isotherms, J. Colloïd Interface Sci. 88 (1982) 36-46.

https://doi.org/10.1016/0021-9797(82)90153-9.

[45] D. Hullmann, G. Wendt, G. Ziegenbalg, Porous Silicon Nitride Materials as Basic Catalysts, Chem. Engineer. Technol. 24 (2001) 147-150. https://doi.org/10.1002/1521-4125(200102)24:2<147::AID-CEAT147>3.0.CO;2-C.

[46] E. P. Parry, An Infrared Study of Pyridi,ne Adsorbed on Acidic Solids. Characterization of Surface Acidity, J. Catal. 2 (1963) 371-379. https://doi.org/10.1016/0021-9517(63)90102-7.

[47] G. Busca, Spectroscopic characterization of the acid properties of metal oxide catalysts, Catal. Today. 41 (1998) 191-206. https://doi.org/10.1016/S0920-5861(98)00049-2.

[48] H. Knözinger, specific poisoning and characterization of catalytically active oxide surfaces, Adv. Catal. 25 (1976) 184-271. https://doi.org/10.1016/S0360-0564(08)60315-6.

[49] Y. Li, W. Zhang, L. Zhang, Q. Yang, Z. Wei, Z. Feng, C. Li, Direct Synthesis of Al−SBA-15 Mesoporous Materials via Hydrolysis-Controlled Approach, J. Phys. Chem. B 108 (2004) 9739-9744. https://doi.org/10.1021/jp049824j